23rd SLOVAK-CZECH-POLISH
OPTICAL CONFERENCE

ON WAVE AND QUANTUM ASPECTS
OF CONTEMPORARY OPTICS

September 02-06, 2024

Hotel Patria****
Štrbské Pleso, Slovakia

The usefulness of different kinds of rotational seismometer in seismological and engineering applications

Leszek R. Jaroszewicz[1,2], Anna Kurzych[1,2]
[1]Institute of Technical Physics, Military University of Technology., 2 gen. S. Kaliskiego Str., Warsaw, Poland
[2]Elproma Elektronika Ltd.,2A Duńska Str.,Czosnów
jarosz@wat.edu.pl

ELPROMA
ELECTRONICS

WAT

Motivation

01 Rotational Seismology

a new, emerging field for the study of all aspects of rotational ground motion induced by earthquakes, explosions, and ambient vibrations [Lee et al. *BSSA*, **99**, (2009) 945-957]

02 Engineering application

seismic behaviour of irregular and complex civil structures [Trifunac, *BSSA*, **99**, (2009), 968-97; Mustafa, InTech, 2015]**, mines activity, wind power monitoring**

03 Seismological application

broadband seismology [Igel et al., *Geophys. J. Int.*, **168**, (2006), 182–197], **strong-motion seismology** [Anderson, 2003, Chap. 57, 937-965], **earthquake physics** [Teisseyre et al. Springer, 2006; Springer, 2008], **seismic hazards** [McGuire, *Earthq. Eng. Struct. D.*, **37**, (2008), 329–338], **seismotectonic's** [www.geophysik.un-muenchen.de/~igel/Lectures/Sedi/sedi_tectnics.ppt], **geodesy** [Carey, Expanding Earth Symposium, (1983), 365-372], **physicists using Earth-based observatories for detecting gravitational waves** [Ju et al., *Rep. Prog. Phys.*, **63**, (2000), 1317–1427; Lantz et al., *BSSA*, **99**, (2009), 980-989]

04 6-DoF

earthquake sources, tilt correction, wavefield separation, wave direction & dispersion, scattering properties, seismic imaging [Murray-Bergquist et al. *Sensors*, **21** (2021), 3732]

[https://www.britannica.com/list/7-women-warriors]

[https://www.businessinsider.com/earthquake-taiwan-east-coast-2018-2?IR=T]

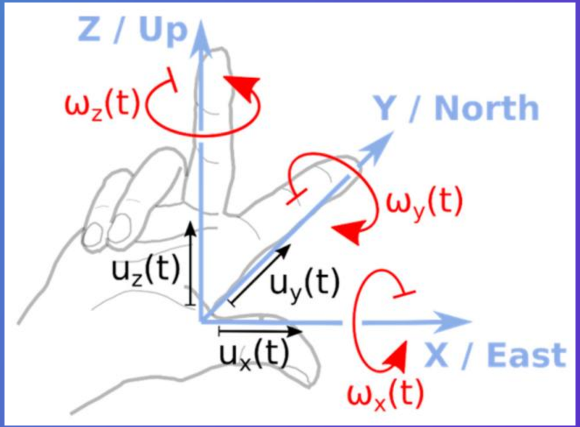

Engineering application

For tall structures, even a tiny rocking motions of the building foundation may matter

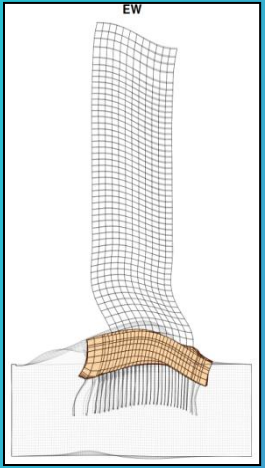

Snapshot of the model of displacement response to an incident plane P-wave half sine displacement pulse with 45° incident angle [Todorovska, WCEE2024 Processing, 2024]

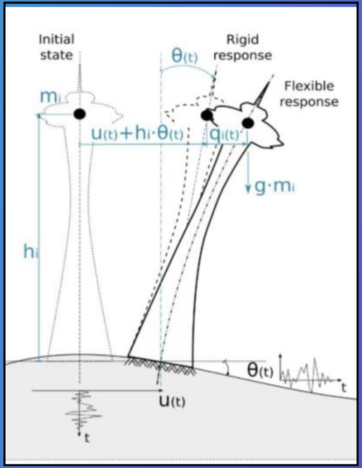

A slender structure under horizontal-rocking ground vibrations [Bońkowski et al., Engineering Structures 155, 387–393, 2018]

Low-frequency content: higher stress in structural element, Horizontal displacement of the center of mass => **Overturning moment**

High-frequency content: meaningless motion of the building centre of mass +> **Local vibration of beams and columns**

[Castellani, Guidotti, 2nd Workshop of IWGoRS Masaryk 's College Prague, (2010)]

Seismological application

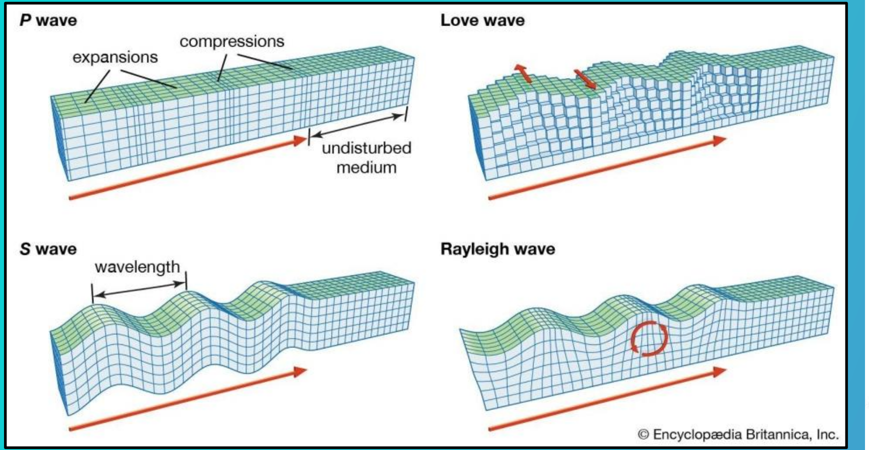

[https://geologyscience.com/natural-hazards/earthquakes/seismic-waves/]

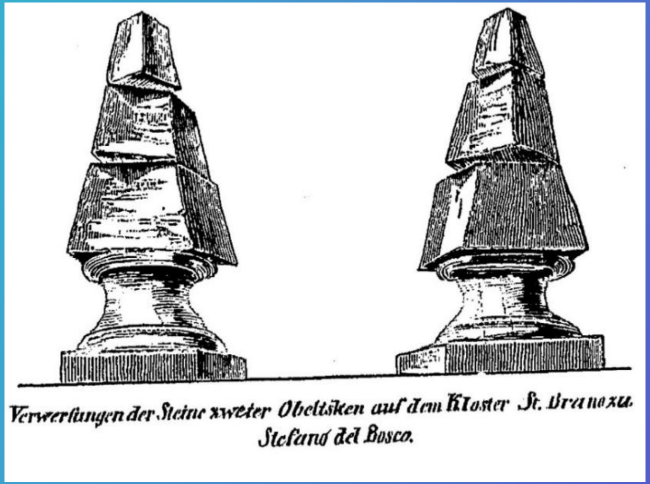

CALABRIA, 05.02.1783

[Gordon et al., *BSSA*, ***60***, 953-971, 1970]

Tombstone in Kushiro Cemetery after the Tokachi-Oki Earthquake 2003

[Hinzen, *J. Seisml*., **16**, (2012), 797–814]

Energy generated during an earthquake propagates not only in the form of linear motions but also in rotational ones.

Earthquakes are undoubtedly one of the most complex phenomena and it is hard to entirely reflect their complexity in theoretical models

Requirements

Engineering application

signal amplitude: up to 10 rad/s,
frequency: 0.01 Hz – 100 Hz

Seismological application

signal amplitude: from 10^{-11} rad/s,
frequency: 0.01 Hz – 0.1 Hz

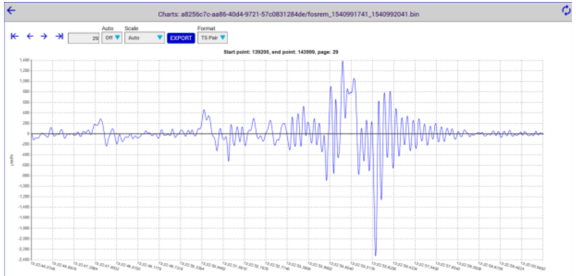

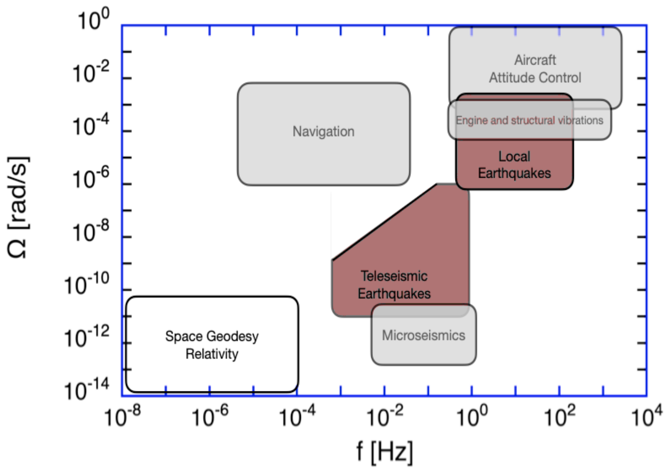

[Schreiber U, Kodet J, WCEE Processing, Milan, Italy 2024]

- Insensitivity to linear motion
- Independent power supply
- Mobility, stability with respect to environmental conditions
- Dynamic range 10^{-8} - 10 rad/s
- Frequency band 0.01 - 100 Hz
- Power consumption 5 – 8 W
- Calibration – in situ (permanently)

ROTATIONAL SEISMOGRAPH

network of seismometers + precise time source + recording device + network

[Bernauer et al., *J. Seismol.*, **16**, (2012)] [Jarozsewicz et al., *Sensors*, **16**, 2161 (2016)]

Real areas of the RS applications:

- Indirect rotation research by numerical conversion
- Rotation effects recording during earthquakes
- Teleseismic waves recordings
- Recordings associated with artificial explosions
- SHM – as examples of engineering application

Indirect recording by numerical conversion

Ref.	Freq. [Hz]	M_w	R [km]	PGV_h [m/s]	PGV_v [m/s]	$PG\omega_z^*$ [μrad]	$PG\omega_z$ [mrad/s]	$PG\omega_x^*$ [μrad]	$PG\omega_x$ [mrad/s]	$PG\omega_y^*$ [μrad]	$PG\omega_y$ [mrad/s]
Bouchon & Aki,1982		6.6	1	1 - 1.6	-	200 - 300	1.2 -1.5	700	-		
Huang, 2003	<1.0	7.6	6	0.33	0.50	171	0.385	44	0.126	177	0.331
Spundich & Flecher, 2008	< 3.6	6.0	8.8	0.25	-	88.1	1.09	68.9	0.925	-	-
		4.7	14.0	0.012		4.69	0.0944	4.74	0.0926		
		5.1	14.4	0.060		20	0.446	0.177	0.372		
		4.9	18.3	0.027		13.6	0.247	9.73	0.215		
Stupazzini, *et al.*, 2009	< 2	6.0	0.02 - 0.90	0.4	0.3	1 690	1	4 000	1.5	1 000	0.6
Wang, *et al* ., 2009	<0.5	7.0	< 80	-	-	-	3.00*		0.350*	-	0.6*
Cao &Mavroeidis , 2019		6.0; 6.4; 7.2; 7.6	1 - 50	<0.72	<0.24	69.2-194.2		16.9-94.3	-	22.7-98.5	-
		6.0; 6.4;7.2; 7.6	1 -50	<0.66	<0.93	54.1-144.3		117.9 - 421.9	-	144.2-325.3	-
Cao &Mavroeidis , 2021	< 1.0	7.5	1 -50	0.11-0.63*	0.03-0.19*	52.6-155*	-	6.2-43.3*	-	10.7-47.4*	-
		6.0	1 -50	0.01-0.23*	0.003-0.045*	5.6-35.5*		2.5-23.1*		1.4-30.7*	
		6.5	1 -50	0.06-0.83*	0.007-0.13*	21-178*		9.7-89*		3.9-29.8*	

PGV_h – peak value of horizontal ground velocity, PGV_v – peak value of vertical ground velocity, $PG\omega_i$ – peak value of rotational velocity around the particular axis.

Panning *et al.* – 6DoF data: compared 3 different conversion methods: the traveling wave, the frequency domain, and the difference one. The first two can convert translational components into rotational ones, but the second shows greater accuracy. However, the last one, although it requires denser reference stations, greatly impacts the accuracy of rotational component calculations.

- Bouchon *et al.* - discrete wave-number representation method, $PG\omega$ ~1.5 mrad/s, $PG\omega_t$ ~0.3 mrad.;
- Huang - numerically integrating accelerograms from a dense acceleration system at the Li-Yu-Tan Dam, $PG\omega$ for each of the 3-axes ranged from 40 to 200 μrad/s;
- Stupazzini *et al.* - 3D numerical modeling to replicate the rotational wave field generated by strike-slip earthquakes in the near field. The assumed $PG\omega_t$ for receivers located on soft ground was ~ one mrad, $PG\omega$ – ten mrad/s;
- Wang *et al.* –finite-difference method - the variability of the hypocenter leads to significant changes in the ground rotation speed;
- Cao & Mavroeidis - finite differential translational motions generated at very closely spaced stations, $PG\omega_t$ ~ 20 to 200 μrad.

Rotation recording during earthquakes

Ref.	ES	Sensor	M_w	R [km]	PGV_h [mm/s]	PGV_v [mm/s]	$PG\omega_z$ [mrad/s]	$PG\omega_x$ [mrad/s]
Takeo, 1998, 2006	strike-slip fault, 1997	Systron Donner triaxial gyro sensor	5.7	3.3	290	500	3.3	26
			5.3	3.3	200	100	8.1	27
Takeo, 2009	seismic swarm at offshore Ito, Japan, 1998		5.0	5.6	100	60	3	6
			3.6	5.9	6	2	0.2	1
			2.4	4.9	6	0.3	0.03	0.2
Liu *et al.* 2009	local earthquakes at the HGSD eastern Taiwan	R-1	5.1	51	-	-	0.63	~0.4
			2.5-6.63	14.3–260.4	-	-	0.004-0.63	-
Brokešová & Málek, 2010	earthquake swarm in Western Bohemia, 2008	Rotaphone 3DOF	2.2	4.4	400	-	0.15	-
Brokešová & Málek, 2013	earthquake at the station Sergoula, Greece	Rotaphone 6DOF	4.3	5	4.5	9	~0.4	~0.8
Yin *et al.*, 2016	215 events at Garner Valley, California, 2008-2014	R-1	3.0-7.2	14-207	-	-	0.006-0.453	-
Jaroszewicz *et al.*, 2017	local earthquake, Jarocin, Poland	TAPS	3.8	200	-	-	0.005	-
		AFORS					0.039	
Ringler *et al.*, 2018	150 local earthquake	Two SMHD (ATA)	4.2	0.5	22.1	11	1.12/0.85	-
			2.8	≤220	-	-	~0.005	~0.00025
			≥ 2.0	≤220			0.0002–2	0.0002–2
Wassermann *et al.*, 2020	volcano-tectonic earthquake	BlueSeis-3A	5.3	1.5	2	1	2.4	2.5
Wassermann *et al.*, 2022	Stromboli volcano, Italy activity	BlueSeis-3A	-	-	<0.01	<0.02	<0.0005	<0.001

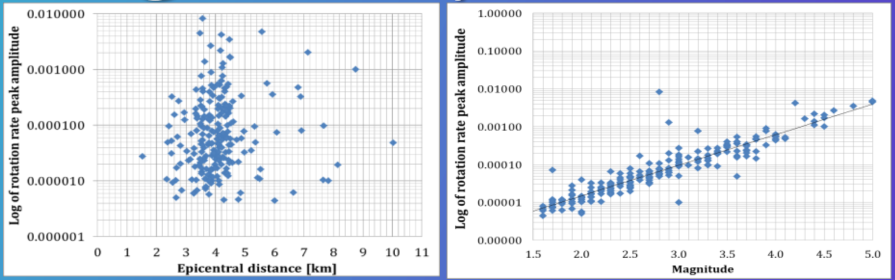

Takeo – 3-axial Gyro (Systron Donner)

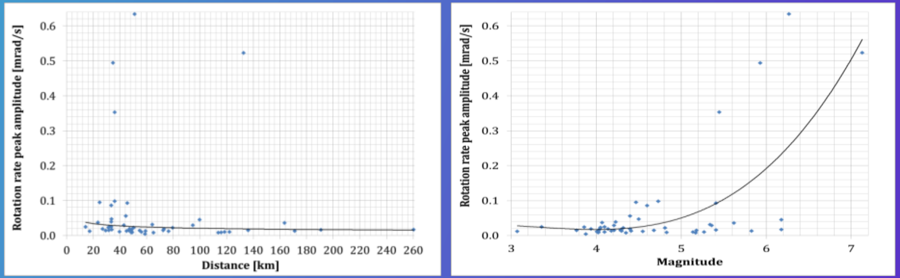

Liu, Yin – R-1 (Eentec)

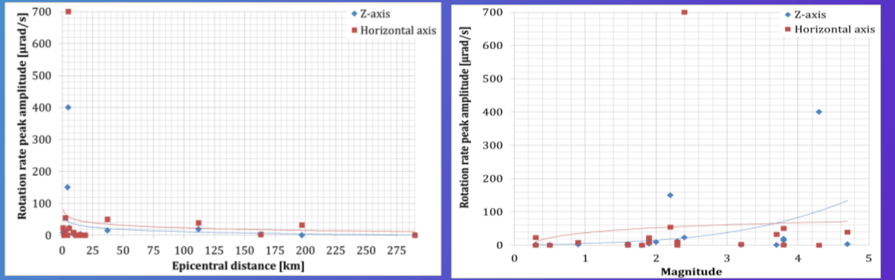

Brokesova – 3DOF, 6DOF Rotaphone (Czech Republic)

Takeda by MEMS gyro: (vibrating tuning fork, vibrating-wheel, resonant wheel, hemispherical resonant, Foucault pendulum apply the Coriolis force to detect the angular velocity) showed that recorded **PGω are several times larger than simulated by Bouchon&Aki based on the dislocation theory.**

Device	3-axial GYRO	TAPS	3DOF	6DOF	D	CY	R-1	AFORS-1	BlueSeis-3A
							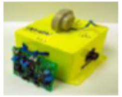		
Year of construction	2008	1998	2010	2012	2015	2019	2006	2010	2017
Sensitivity [nrad/s]	no data	100	16.7	2.16	3.77	0.042	1200	4	20
$\Omega_{Max.}$ [mrad/s]	873	100	10	287	31.7	31.68	0.1	64.3	0.1
Dynamic range [dB]	no data	120	100	120	120	120	110	124	135
Frequency range [Hz]	DC - 75	0.7 – 50	1 – 100	2 – 60	2 – 80	1–100	0.05 - 20	0.83-106	DC - 100
Sampling rate	no data	100	250	250	250	250	N/A	212	up to 200
Sensors: [No. x type]	MEMS	2 x SM-3	8 x LF-24	9; 12 SM-6	16 x SM-6	12 x SM-6	fluid MET	optical	optical
Eigen frequency	no data	45	1	4.5	4.5	4.5	N/A	N/A	N/A
Spacing of sensors [m]	N/A	0.28	0.3	0.3	0.4	0.3	N/A	N/A	N/A
Operating temp. [°C]	< 125	-10 – +45	-20 – +40	-20 – +40	-20 – +100	-40 – +70	-15 – +55	-10 – +50	-10 – +50
Weight [kg]	0.3	15	4.5	9.5	15.3	22	1.0	18	20
Dimensions [LxWxH] [cm]	no data	45x18x35	25* x 1	35x30x43	44.5x12	55*x50	12x12x9	70* x 16	30*x60

* diameter

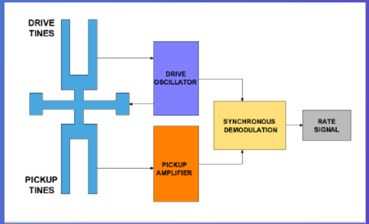

MEMS - vibrating tuning fork, vibrating-wheel, resonant wheel, hemispherical resonant, Foucault pendulum apply the Coriolis force to detect the angular velocity

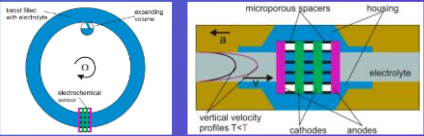

R-1 (R-2) - no flat above 1 Hz, 80 dB instead declare 110 dB, 27% (R-1) and 18% (R-2) signal deviation in temp. +20 - +50 C.

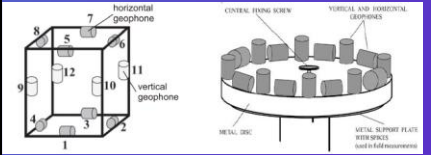

Rotaphone (3DOF, 6DOF, D) Ω is determined by more accurately as result of more than one geophone pair; frequency ranges are still too narrow

AFORS-1 (uniaxial), BlueSiei-3A (triaxial) optical system based on (or uses) FOG – physically the Sagnac effect in fiber-optic loop interferometer, mass-free (non-inertial) system **-> probably the best solution for rotational seismograph fulfill all RS requirements.**

BACKGROUND

The direct utilization of the Sagnac effect

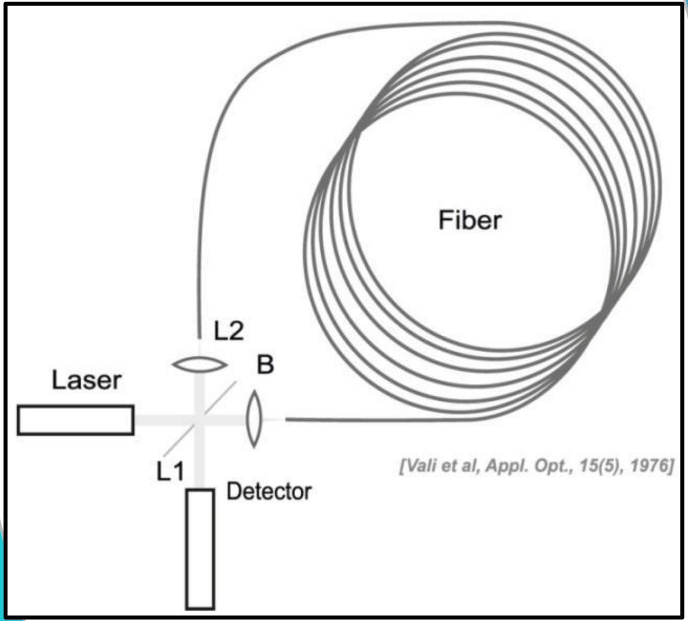

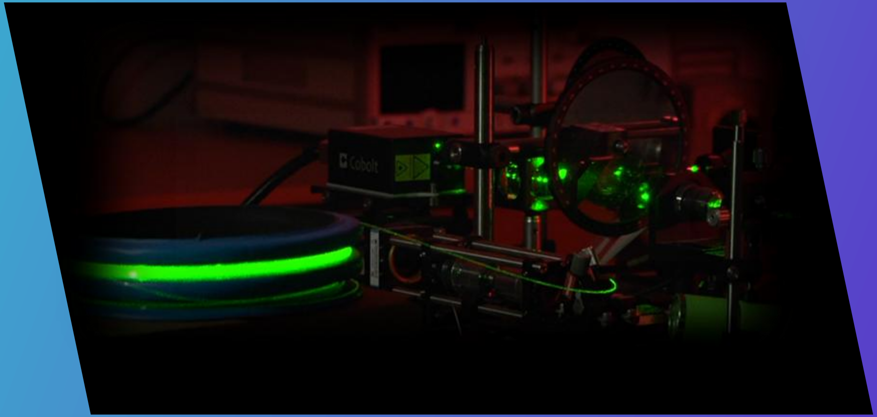

Sagnac effect (1913) shows the difference between phase of two beams propagating around closed optical path, in opposite direction when this path is rotating with rotational rate Ω.

In a fibre-optic implementation (1978) the rotation rate Ω is expressed by induced phase shift Δφ as:

$$\Omega = S_o \cdot \Delta\varphi = \frac{\lambda c}{4\pi RL} \cdot \Delta\varphi$$

L – length of the fiber in the sensor loop, *R* – sensor loop radius, *λ* – wavelength of used source, *c* – velocity of the light in vacuum, S_0 – the optical constant of an interferometer

Teleseismic waves recording

Ref.	ES	Sensor	M_w	R [km]	PGV_h [m/s]	$PG\omega_z$ [nrad/s]	$PG\omega_x$ [nrad/s]	$PG\omega_y$ [nrad/s]
Pancha *et al*. 2000	New Ireland, 1999	C-II, G0	7.0	~4 700	-	10 (C-II)	5 (G0)	-
	Vanuatu, 1999	C-II	7.3	~3 500		8	-	
Igel *et al*. 2005	Thrust Japan	G-ring	8.1	~8 830		~35		
Igel *et al*. 2007	Germany to Great Andaman	G-ring	5 - 9	370–12 700	-	~0.10 –40	-	-
Schreiber *et al*. 2009	Kamachatka, 2006	GEOsensor	7.6	~6 500	5 197	~10	-	-
	Mexico, 2006		5.4	~2 000	4 646	~5		
	California, 2007		3.6	~200	8 670	~16		
	California, 2007		3.9	~250	14 512	~30		
Belfi *et al*. 2012	Japan, 2011	G-Pisa	9.0	-	-	~60	-	-
Ross *et al.* 2017	Papua New Guinea, 2016	BRS beam rotation sensor	7.9	-	$\sim150\cdot10^{-6}$	-		~30
	Vanuatu, 2016		6.7		$\sim6\cdot10^{-6}$			~2
	New Caledonia, 2016		7.2		$\sim40\cdot10^{-6}$			~10
	North of Ascension Island, 2016		7.1		$\sim15\cdot10^{-6}$			~4.5
	New Zealand, 2016		7.8		$\sim200\cdot10^{-6}$			~60
	Papua New Guinea, 2017		7.9		$\sim150\cdot10^{-6}$			~30
Simonelli *et al*. 2018	Series in Italy, 2016	GINGERino	3.5–5.9	38 -77	-	~600–17 000	-	-
Sollberger *et al.* 2020	Gulf of Alaska, 2018	ROMY	7.9	-	-	~6	~8	~4
Igel *et al*. 2021	Papua New Guinea, 2019	ROMY	7.6	14 000	-	~8.5	~9	-
	Turkey, 2019		5.7	1 500		~5	~9	
	Austria, 2018		3.8	144		~18.9	~18	

- strong earthquakes
- extrmely distance R
- extremely low PGω (nrad/s) amplitude

GINGERino

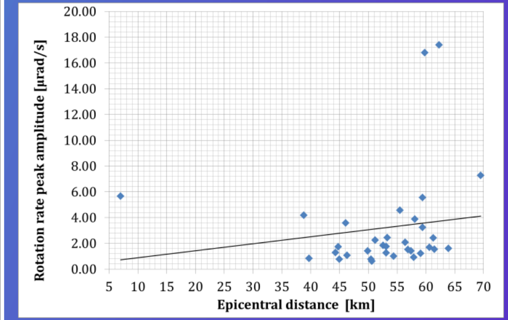

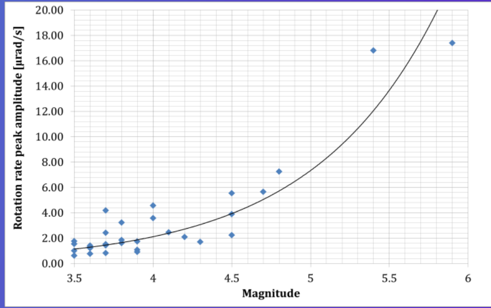

Name	C-I	C-II	G-0	G	UG1	UG2	UG3
							
Year	1992/2011	1997/2011	1998/2011	2001	201/2011	2004/2011	2009
Place	Cashmere, New Zealand			Wettzell, GE	Cashmere, New Zealand		
Area [m^2]	0.748 (0.85 m square	1	12.25 (3.55 m square	16.0 (4.0 m square	367.5 (17.5x 21)	833.7 (1.0 x 39.7)	367 (7.5x 21)
Perimeter	3.48 m	4.0 m	14 m	16 m	77 m	121.4 m	77 m
Sensitivity [nrad/s/√Hz]	no data	0.146	0.0116	0.012	0.0171	0.0078	no data
$\Delta\Omega/\Omega_E$	no data	$1 \cdot 10^{-6}$	$5 \cdot 10^{-6}$	$3.4 \cdot 10^{-8}$	$3 \cdot 10^{-8}$	$2 \cdot 10^{-8}$	no data
Name	**PR-1**	**GEOsensor**	**G-Pisa**	**GINGERino**	**PP-2**	**ROMY**	
			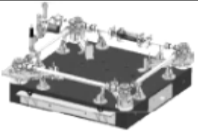		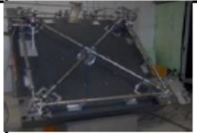		
Year	2004	2005	2008	2014	2014	2016	
Place	Cashmere	California	Pisa, Italy			Furstenfeldburck, Germany	
Area [m^2]	2.56 (1.6 m square	2.56 (1.6 m square	1.96 (0.9x0.9 to 1.4x1.4)	12.96	2.56	72 -3 vertical 50- horizontal	
Primeter	6.4 m	6.4 m	5.4 m	14 m	6.4 m	36 m; 30 m	
Sensitivity [nrad/s/√Hz]	1.5	0.108	~1.0	0.1	2	0.08 - 1.0	
$\Delta\Omega/\Omega_E$	$8.5 \cdot 10^{-4}$	$1 \cdot 10^{-7}$	$2 \cdot 10^{-5}$	$\sim 10^{-6}$	$\sim 6 \cdot 10^{-5}$	$5 \cdot 10^{-5}$	

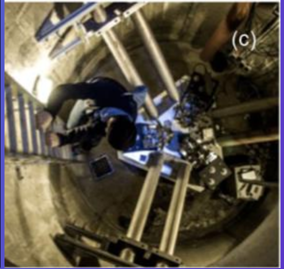

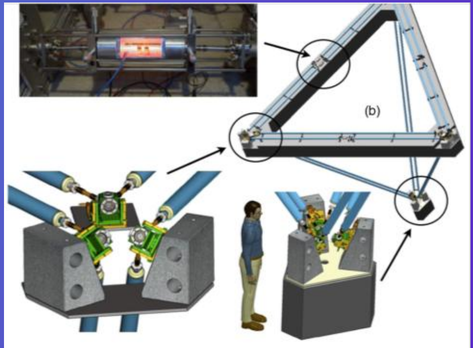

ROMY – ROtational Motion in seismologY

Recordings associated with artificial explosions

Ref.	VS	Sensor	R [km]	$PG\omega_z$ [mrad/s]	$PG\omega_x$ [mrad/s]	$PG\omega_y$ [mrad/s]
Nigbor 1994	1 kT chemical explosion at the Nevada Test Site	QRS11	1	-	38	-
Wasserman *et al*. 2009	Demolition blast of building in Munich, Germany	R-1	0.2	0.02	0.008	0.05
Lin *et al*. 2009	3000 kg explosives,	R-1	0.2539–0.6082	0.268-0.966	0.370-2.741	0.627-2.524
	750 kg explosives, TAIGER experiment, Tawian			0.301-0.563	0.235-1.750	0.394-1.185
Brokešová & Málek 2013	medium-size quarry blast, 3044 kg explosive, Czech	6 DOF Rotaphone	0.362	~1	~4.5	~2
Barak *et al.* 2018	Ignition of Betsy gun at Silver Lake, California	METR-03	<1	-	<0.1	<0.2
Kurzych *et al.* 2019 Teisseyre *et al.* 2019	Digging shafts with the multiple blasts technique, Książ, Poland	FOSREM, TAPS, RS.LQ–RP/P	0.075	0.05-1	-	-
Bernauer *et al.* 2021 Kurzych *et al.* 2021	500 g explosive, Fürstenfeldbruck, Germany	BlueSeis-3A, FOSREM, ROMY, Rotaphone-CY, FARO, PHINS, Quadrans, MEMS (Horizon, Gladiator)	~0.05	~0.5 (BlueSeis-3A) ~1 (FOS5-01) ~0.5 (FOS5-02) <0.5* (BlueSeis-3A) ~0.005* (ROMY) <0.02* (FARO) <0.025*(FOS5) ~0.025* (PHINS) < 0.025*(Quadrans) <0.05 *(Rotaphone)	<0.1* (BlueSeis-3A) <0.15* (PHINS) < 0.1* (Quadrans) <0.09* (Rotaphone)	~0.1-0.15 (BlueSeis-3A) <0.15 (PHINS) <0.15 (Rotaphone) <0.15* (BlueSeis-3A) ~0.15* (PHINS) < 0.15*(Quadrans) <0.15 *(Rotaphone)
	VibroSeis truck, Fürstenfeldbruck, Germany	FOS5-1	0.096	0.0177	-	-
			0.105	0.0252		
			0.113	0.0386		
			0.121	0.0158		
			0.130	0.0156		
			0.138	0.0141		
Cao *et al*. 2021	near field explosion, China	RotSensor3C	0.150	~11	~11	~16
Brokešová & MáleK 2022	medium-size blast at the Klecany quarry, Czech Republic	Rotaphone, R-1, ADR (array-derived-rotation)	0.240	~0.05 (Rotaphone) ~0.01 (R-1) ~0.05 (ADR)	~0.25(Rotaphone) ~0.1 (R-1) ~0.25 (ADR)	~0.15 (Rotaphone) ~0.03 (R-1) ~0.1 (ADR)
				~0.05 (Rotaphone) ~0.03 (R-1) ~0.06 (ADR)	~0.25 (Rotaphone) ~0.2 (R-1) ~0.22 (ADR)	~0.2 (Rotaphone) ~0.08 (R-1) ~0.1 (ADR)

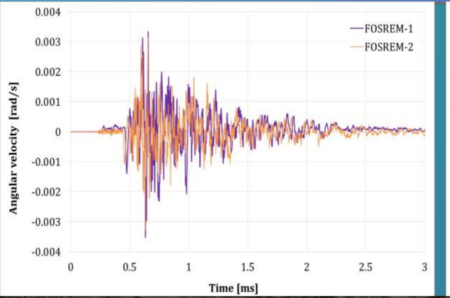

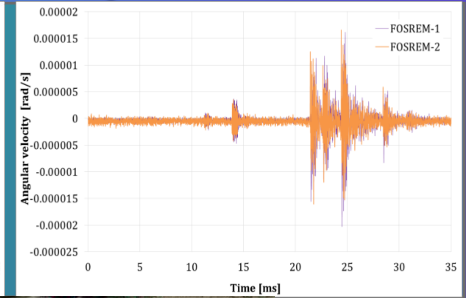

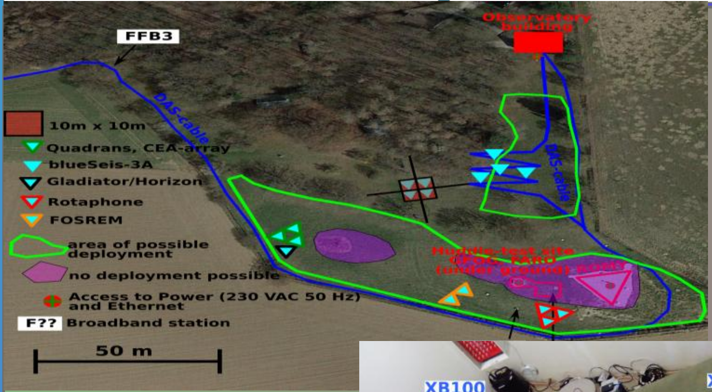

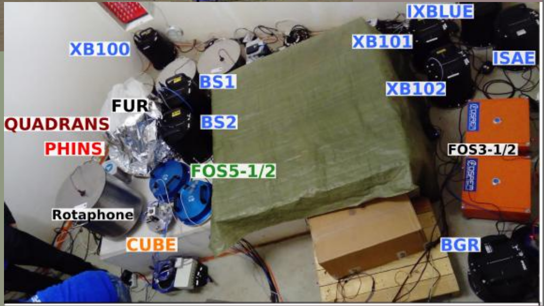

Experiment Fürstenfeldbruck 19-22.11.2019

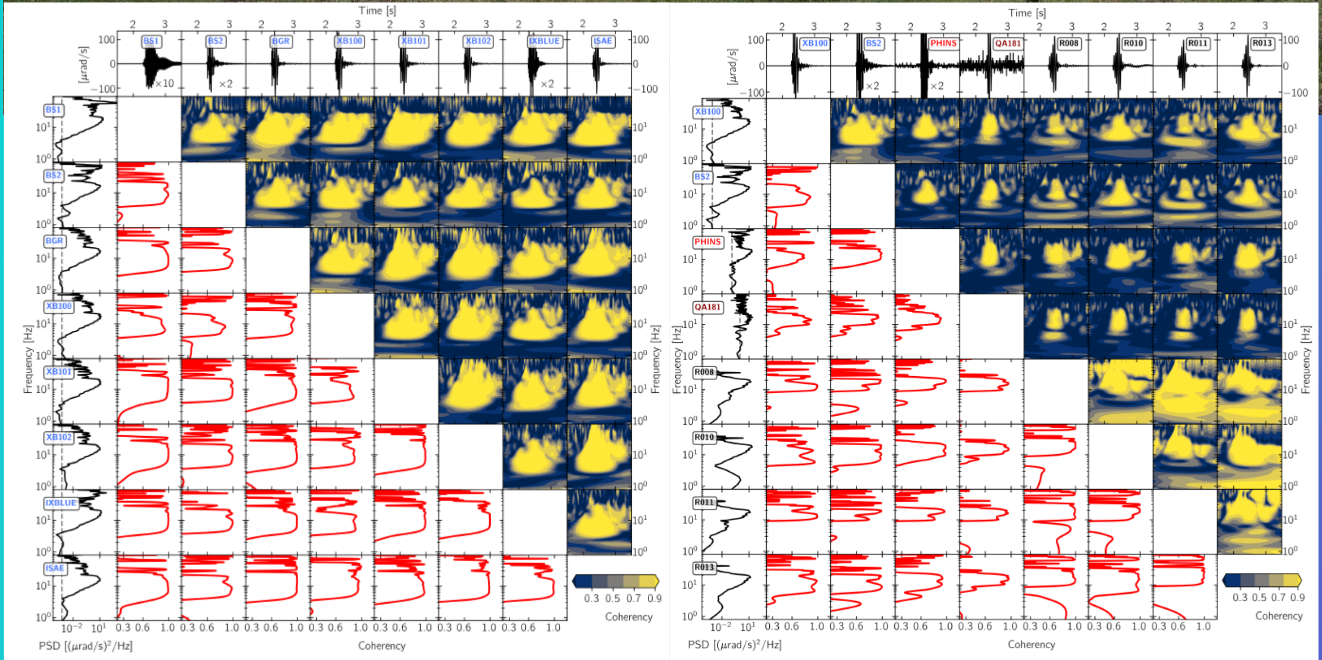

6th Meeting IWGoRS
23-25.11.2022 Paris:
More than 150 axes manufactured,
40 units in the world today

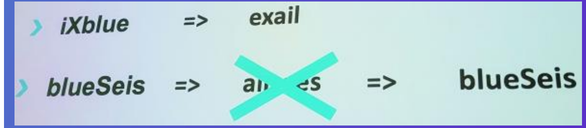

eaxil does not have blueSeis in its offer TODAY !!!

FOSRREM in FOS6 configuration from Elproma Electronics

Fibre-Optic Rotational Seismograph historical brief

1998

GS-13P
Ω_{min}: $3.49 \cdot 10^{-3}$ rad/s
SL: 380 m PANDA
Radius: 0.1 m
ΔB: DC – 100 Hz

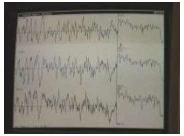

2001

FORS-I
Ω_{min}: $2.2 \cdot 10^{-6}$ rad/s
Ω_{max}: $4.8 \cdot 10^{-4}$ rad/s
SL: 400 m PANDA
Radius: 0.1 m
ΔB: DC – 100 Hz

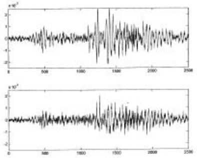

2004,2010

FORS-II (FOS1)
Ω_{min}: $4.2 \cdot 10^{-8}$ rad/s
Ω_{max}: $4.8 \cdot 10^{-4}$ rad/s;
SL: 11 000 m SMF
Radius: 0.34 m

AFORS (FOS2)
Ω_{min}: $4 \cdot 10^{-9}$ rad/s,
Ω_{max}: $6.4 \cdot 10^{-3}$ rad/s
SL: 15 000 m SMF
Radius: 0.34 m ΔB: 0.83– 06 Hz

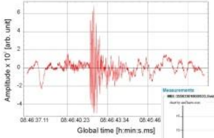

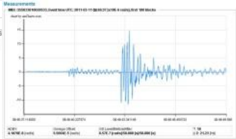

2015

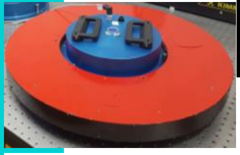

FOS5-04
Ω_{min}: $1.1 \cdot 10^{-9}$ rad/s,
Ω_{max}: 10 rad/s
SL: 14 400 m SMF,
Radius: 0.305 m
ΔB: DC – 100 Hz

FOSREM (FOS3 & FOS4)
Ω_{min}: $2 \cdot 10^{-8}$ rad/s,
Ω_{max}: few rad/s
SL: 5 000 m SMF
Radius: 0.125 m ΔB: DC–328 Hz

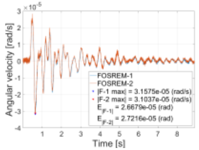

2019

FOS5-0# (3=1,..,)
Ω_{min}: $7 \cdot 10^{-8}$ rad/s,
Ω_{max}: 10 rad/s
SL: 5 000 m SMF,
Radius: 0.125 m

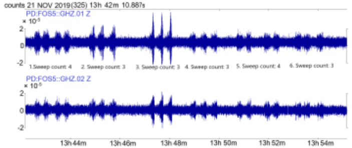

2023

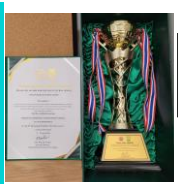

FOSREM (FOS6)
3- Axis with 100 ns time synchronization
Ω_{min}: 35 nrad/s
Ω_{max}: 10 rad/s
SL: 6 000 m SMF
Radius: 0.125 m
Weight: 10 kg, ΔB: DC – 100 Hz

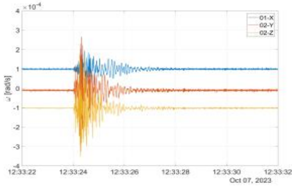

Fibre-Optic Seismograph

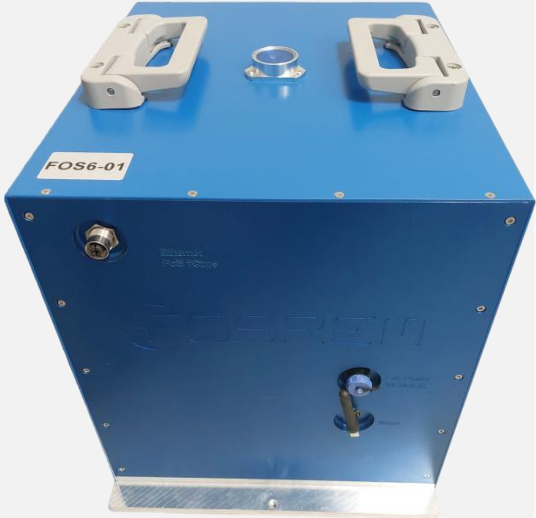

OPTICAL PART

generates the phase shift Δφ proportional to the measured rotation rate Ω which is perpendicular to the sensor loop plane

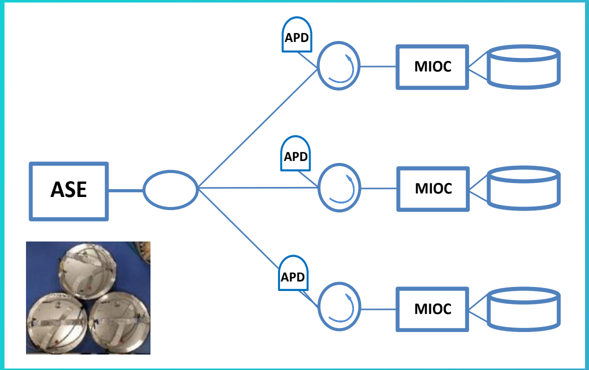

ELECTRONIC PART

enables to calculate and record information about rotational motions via digital closed-loop signal processing

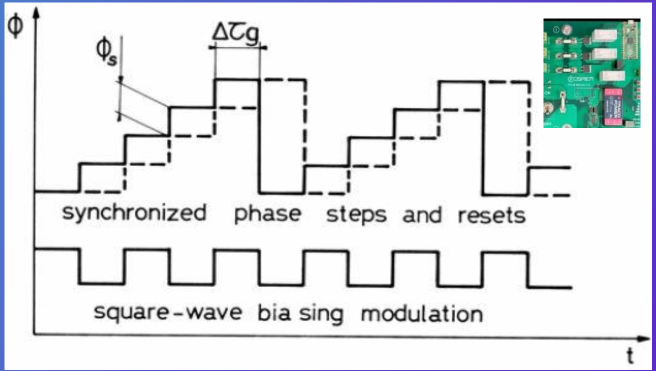

Laboratory analysis of FORS' parameters

Allan Variance analysis

Theoretically

$$S = \frac{\sqrt{2}\lambda c}{2\pi D L}\sqrt{\frac{4kT}{R\eta^2 P^2}+\frac{e i_d}{\eta^2 P^2}+\frac{e}{\eta P}+\frac{\lambda^2}{4c\Delta\lambda}} \equiv_{|\Delta B=1\text{Hz}} \text{ARW}$$

where: λ – central light wavelength (1 550 nm), c – speed of light, D – loop diameter (0.25 m), L – loop length (about 6 000 m), k – Boltzmann's constant, T – temperature (293 K), R – resistance of the trans-impedance transducer of the photodetector device (20 kΩ), η – efficiency ratio of the photodiode (0.85 A/W), P – incident optical power on the APD, e – elementary charge, i_d – photodiode dark current (80 nA), $\Delta\lambda$ – spectral width of the light source (40 nm).

The calculated theoretical values of ARW for each optical head for four FORS type FOS6 were in the range of **4.49-4.85 nrad/s√Hz**, depending on total optical losses and fiber length in the given optical head.

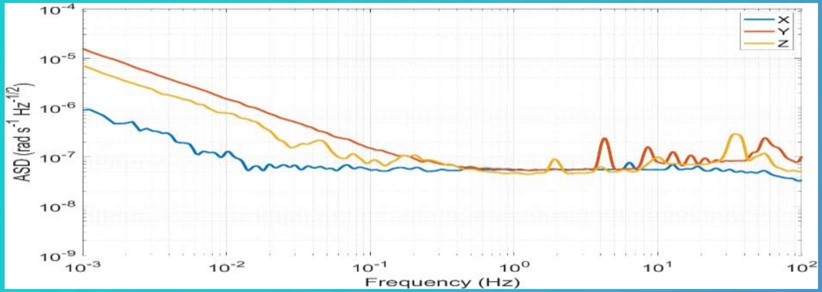

Allan Variance analysis

Data gathered in the Military University of Technology, Poland as Autonomous Rresion Metod for Allan Variance (ARMAV) [Jurando, et al., *Navigation*, **66** (2019), 1-13]

ADEV(t)=√AVAR(t) ➔ ASD instead of PDS

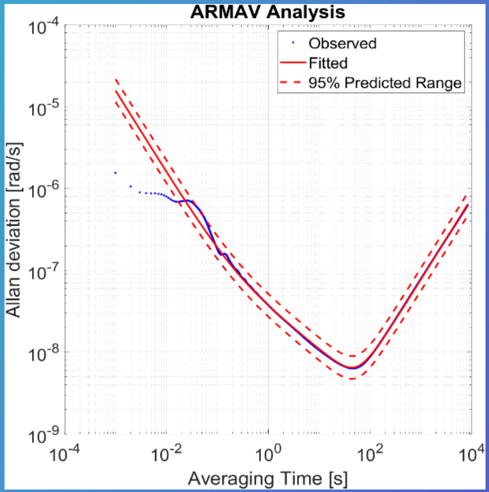

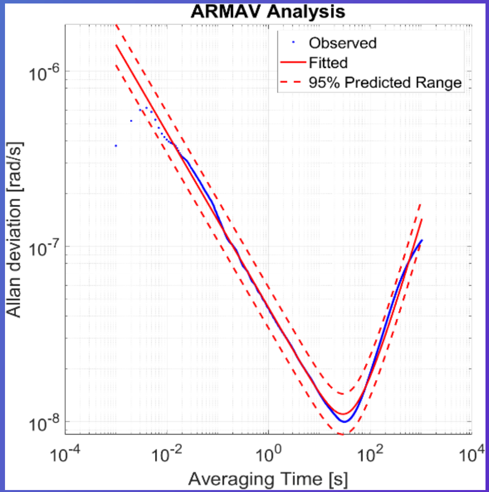

FOS6-01: ARW: 35 nrad/s/√Hz, BI: 10.0 nrad/s

FOS6-02: ARW: 45 nrad/s/√Hz, BI: 15.0 nrad/s

FOSREM as FOS remote controls by webpage

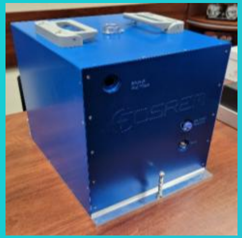

System control

Paramters change

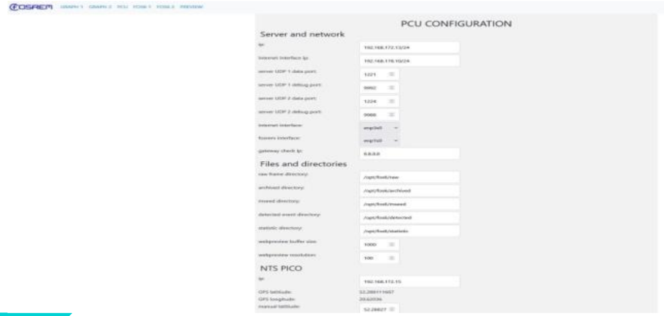

Data downloading

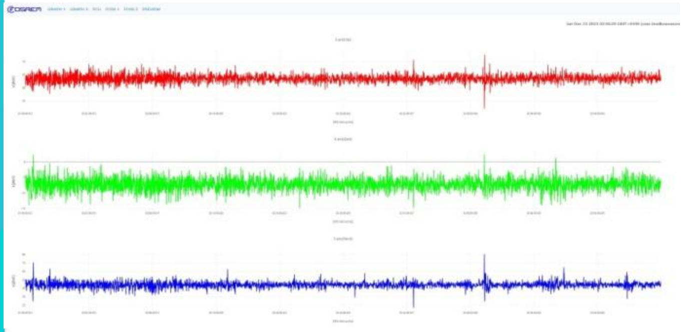

Localization

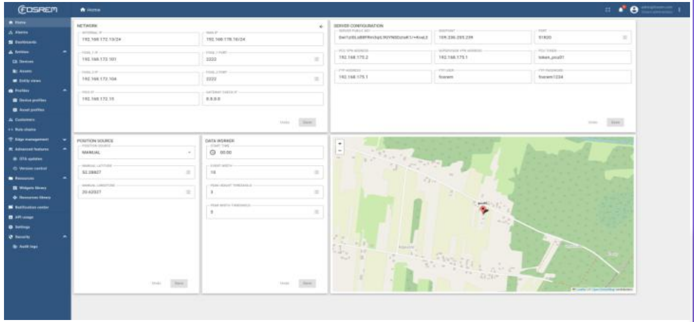

Correlation verification

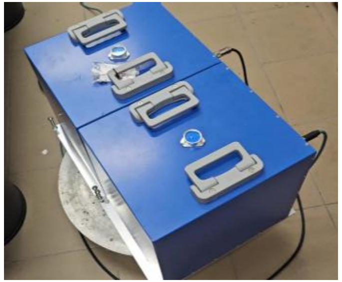


FOS6-01 and FOS6-02 in the MUT laboratory on the rotary table


Field test in the Kampinos Nature Park by a pair of FORSs (FOS6-01 and FOS6-04)

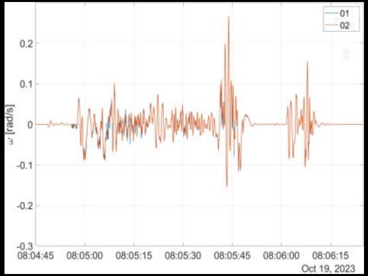

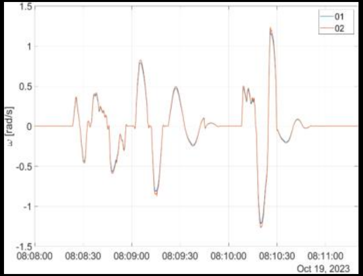

Signals recorded by FORSs Z-axes during the medium high-amplitude and fast-changing excitations as well as high-amplitude amplitude excitations

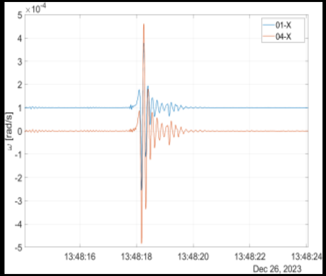

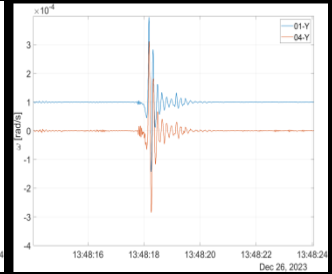

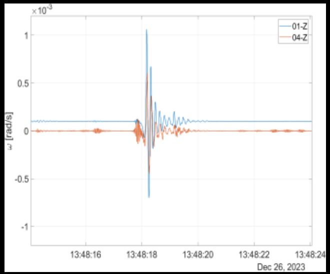

A weak rotational disturbance recording (with an amplitude of about 0.5 mrad/s) generated by the wild animal (elk) moving in the field close to the FORSs location

Pearson correlation coefficient equal to 99.42% and 99.99 %

Pearson correlation of about 95% for the X axis, about 99% for Y axis, and about 99% for the Z axis

Rotation Detection During Detonation of na Explosive Charge

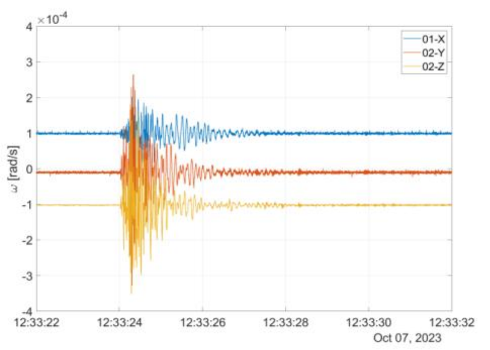

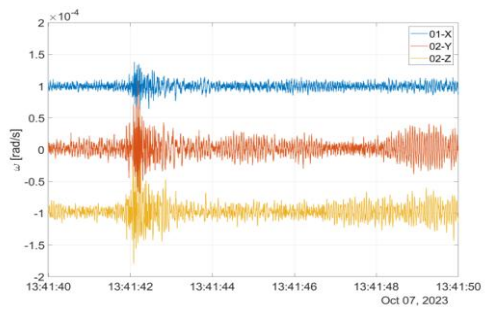

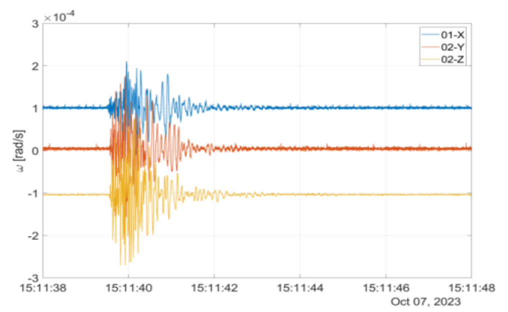

On the 7th of October 2023 there were three explosions performed:

1. 12:33 UTC, 5 kg of explosive, 3 m below the ground surface with surface discharge.
2. 13:41 UTC, 5 kg of explosive, 4.5 m below the ground surface without surface discharge.
3. 15:11 UTC, two 5 kg explosive charges installed 5 meters apart were detonated one after the other, 4.5 m below the ground surface, with a distance of 5 m between loads.

	A_{max} [μrad/s]			E_f [μrad]		
Explosion number/ Axis of FORS	X	Y	Z	X	Y	Z
Explosion 1	140	327	281	69	163	104
Explosion 2	38	108	83	41	98	94
Explosion 3	119	177	170	65	111	106

Thank You For Your Attention

STATUTORY ACTIVITY
the Military University of Technology
Grant UGB 725

FOSREM - FROM SKY ACROSS GROUND UP TO UNDERGROUND
National Centre for Research and Development project POIR.01.01.01-00-1553/20-00

FOM-MEM - FIBRE-OPTIC MATRIX FOR MECHANICAL EVENTS MAPPING
Polish Agency for Enterprise Development project FENG.01.01-IP.02-1714/23